UNIVERSAL SHARPENING-DEMOSAICING FOR VARIOUS TYPES OF COLOR-FILTER ARRAY

Takashi Komatsu and Takahiro Saito

Department of Electronics & Informatics Frontiers, Kanagawa University
3-27-1 Rokkakubashi, Kanagawa-ku, 221-8686, Yokohama, Japan
phone: + (81) 45 481 5661, fax: + (81) 45 491 7915, email: saitot01@kanagawa-u.ac.jp
web: http://slat4.ee.kanagawa-u.ac.jp

ABSTRACT

A monochrome-image iterative deblurring method with the classic soft-shrinkage in the shift-invariant Haar wavelet transform domain was recently proposed by R. H. Chan et al. Extending this deblurring method, we present a new iterative sharpening-demosaicing method with the shift-invariant Haar wavelet transform and our color shrinkage utilizing redundant color transform. Our new sharpening-demosaicing method is originally constructed for the Bayer's primary color-filter array (CFA), but its minor modification renders it applicable to various CFA's other than the Bayer's CFA: the complementary CFA, the random arrangement CFA, and so on. Simulation results demonstrate that our new sharpening-demosaicing method in the shift-invariant Haar wavelet transform domain works much more efficiently than our previously proposed sharpening-demosaicing method with the total-variation regularization in the spatial image-domain.

1. INTRODUCTION

To suppress aliasing artifacts caused by the color mosaicing with a color-filter array (CFA), a digital color camera uses an optical low-pass filter (O-LPF). As side effects of the O-LPF, observed color data have been blurred. To recover a sharp color image, we need an advanced demosaicing method which performs color interpolation and deblurring, simultaneously. Along this line, previously we have proposed the iterative sharpening-demosaicing method with the classic total-variation (TV) regularization in the spatial image-domain [1]. On the other hand, recently, R. H. Chan et al. have proposed a monochrome-image iterative deblurring method with the classic soft-shrinkage in the shift-invariant Haar wavelet transform domain, and their method successfully deblurs a monochrome image [2]. This paper extends their method to the sharpening-demosaicing for a digital color camera. Our new iterative sharpening-demosaicing method employs our color shrinkage utilizing redundant color transform [3], instead of the classic soft-shrinkage.

Firstly we present an algorithm for the sharpening-demosaicing for the primary CFA such as the Bayer's CFA, and then modify the algorithm for the complementary CFA. Moreover, we experimentally compare various CFA'*s* [4]~[6] from the standpoint of quality of color images restored by our sharpening-demosaicing method.

2. DEBLURRING IN THE SHIFT-INVARIANT HAAR WAVELET TRANSFORM DOMAIN

The 2D shift-invariant Haar wavelet transform (SI-HWT) with one resolution layer decomposes an input image into its four frequency bands: the LL, LH, HL and HH bands. The LL band consists of its scaling coefficients, each of which is equal to double the average of its four neighboring pixels, and the LL band corresponds to a blurred version of the input image. The forward SI-HWT is regarded as a blurring operator, whereas the inverse SI-HWT corresponds to a deblurring operator. Given wavelet coefficients, compatible with the scaling coefficients in the LL band identical to double the blurry input image, then the inverse SI-HWT will produce a deblurred image. Therefore, the key to the deblurring is how to recover those compatible wavelet coefficients. In the SI-HWT, its LL, LH, HL, and HH bands are mutually dependent, and hence the wavelet coefficients in those bands are not determined separately. Utilizing this interdependence will enable us to recover wavelet coefficients compatible with the scaling coefficients given by the blurred input image.

Along the above-mentioned line, R. H. Chan et al. have recently proposed an iterative deblurring method with the SI-HWT and the classic soft-shrinkage [2]. The concept of their iterative deblurring method is as follow. If the LL band is replaced by double the blurry input image and the wavelet coefficients of the other bands are set to zero, the inverse SI-HWT will produce a provisionally-restored image. Subsequently, if the forward SI-HWT is applied to this restored image, all the bands will be updated; the updated LL band will not necessarily be identical to double the blurry input image, and the LH, HL, and HH bands will be given none zero values. Through the iteration of the pair of the inverse and the forward SI-HWT along with the replacement of the LL band by double the blurry input image, the LH, HL, and HH bands are gradually recovered to be compatible with the LL band. However, since there are infinite solutions of the compatible wavelet coefficients, this iterative deblurring problem is an ill-posed inverse problem. To stabilize the iterative deblurring process, a certain norm of the wavelet coefficients in the bands to be recovered should be minimized. Along this line, R. H. Chan et al. applies the classic soft-shrinkage to the wavelet coefficients, to minimize the Besov norm of the wavelet coefficients. The Besov norm is defined as the sum of the l^1 norm of the wavelet coefficients, and well approximates the TV norm [7]. Therefore, the soft shrinkage in the wavelet transform domain achieves desirable image-recovery from the standpoint of the sparse image-representation.

The algorithm of the iterative deblurring method proposed by R. H. Chan et al. is as follows.

[Iterative Deblurring Algorithm in the SI-HWT Domain]

1) The LH, HL, and HH bands are initially set to zero.
2) The LL band is replaced by double the blurry input image.
3) The soft shrinkage is applied to all the wavelet coefficients in the LH, HL, and HH bands.
4) The inverse SI-HWT is applied to all the bands to produce a restored image.
5) The forward SI-HWT is applied to the restored image provided at the step 4).
6) Return to the step 2).

[End of the algorithm]

3. OPTICAL LOW-PASS FILTER (O-LPF) AND THE SIFT-INVARIANT HAAR WAVELET TRANSFORM (SI-HWT)

A digital color camera uses doubly-refractive crystal devices as the O-LPF. This device decomposes a ray of incident light into two outgoing rays: the ordinary ray and the extraordinary ray. If we use the doubly-refractive crystal device so that the distance of the two outgoing rays can coincide with the pixel interval of an imaging device, then the crystal device will perform an averaging operation of two neighboring pixels. To accomplish desirable low-pass filtering, vertically and horizontally directional doubly-refractive crystal devices are combined. This combination achieves the 2 by 2 averaging filtering shown in Fig. 2(a). The image captured through this O-LPF corresponds to the scaling coefficients of the LL band provided by the SI-HWT with one resolution layer. The combination of the two vertical and the two horizontal crystal devices achieves the 3 by 3 low-pass filtering shown in Fig. 2(b). The combination of a horizontal device and a vertical one corresponds to the single-layer Haar smoothing filter, whereas the combination of two vertical and two horizontal devices corresponds to the two-layer Haar smoothing filter, in which unlike the usual Haar smoothing filter, the second layer employs the same Haar smoothing filter as that used at the first layer. A digital color camera uses an O-LPF with the characteristics ranging from Fig. 2(a) to Fig. 2(b). It stands to reason that the deblurring algorithm in the SI-HWT domain should be extended to a sharpening-demosaicing algorithm.

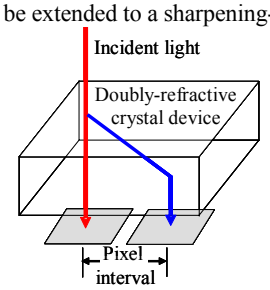

Figure 1 – Doubly-refractive crystal device.

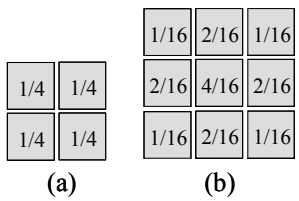

Figure 2 – Averaging filtering of the two O-LPF's.

4. ITERATIVE SHARPENING-DEMOSAICING METHOD

Extending the iterative deblurring method of R. H. Chan et al. [2], firstly we construct an iterative algorithm of the sharpening-demosaicing for the primary CFA such as the Bayer's CFA, and then we extend our iterative algorithm to an algorithm of the sharpening-demosaicing for the complementary CFA.

4.1 Algorithm for the primary CFA

The outline of our iterative sharpening-demosaicing method for the primary CFA is shown in Fig. 3, where the three leftmost rectangles painted RGB represent a demosaicked color image. The L_1L_1, L_1H_1, H_1L_1 and H_1H_1 bands represent the first layer of the SI-HWT of the RGB components of the demosaicked color image, respectively. The L_2L_2, L_2H_2, H_2L_2 and H_2H_2 bands represent the second layer of the SI-HWT, whereas the L_3L_3, L_3H_3, H_3L_3 and H_3H_3 bands represent the third layer of the SI-HWT. The purple and the orange arrows show the inverse and the forward SI-HWT, respectively. The top mosaicked rectangle represents a mosaicked raw color data captured by an image sensor with the Bayer's CFA. The red broken frame means that the color shrinkage in a redundant color space is applied to the wavelet coefficients in the enclosed nine bands: the L_1H_1, H_1L_1, H_1H_1, L_2H_2, H_2L_2, H_2H_2, L_3H_3, H_3L_3 and H_3H_3 bands. Our algorithm presumes the O-LPF of Fig. 1(a) and employs the three-layer SI-HWT.

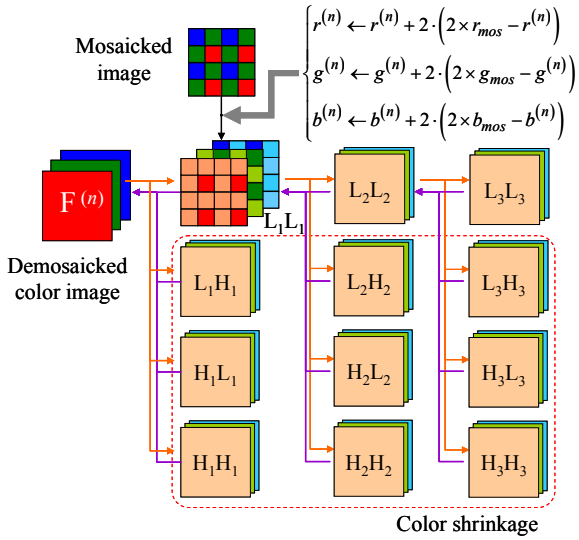

Figure 3 – Iterative algorithm of the sharpening-demosaicing for the primary CFA.

The iterative algorithm of our sharpening-demosaicing approach is as follows.

[Algorithm of Our Iterative Sharpening-Demosaicing Approach]

1) Initial setting:

We set the iteration parameter n to 1. We initialize the demosaicked color image $\mathbf{F}^{(0)}$ to be null. We initialize the scaling coefficients in the band $L_1L_1^{(1)}$ and the wavelet coefficients in the three bands, $L_1H_1^{(1)}$, $H_1L_1^{(1)}$, $H_1H_1^{(1)}$, to be zero. We set the threshold parameter T_h used for the convergence test and the two maximum values, μ_+, μ_-, of the threshold parameters used by the color shrinkage in a redundant color space. We proceed to the step 7).

2) Color shrinkage of wavelet coefficients:

We apply the color shrinkage with redundant color transform [3] to all the wavelet coefficients in nine bands, $\{L_mH_m^{(n)}, H_mL_m^{(n)}, H_mH_m^{(n)} \mid m = 1, 2, 3\}$. Firstly we transform a triplet (r, g, b) of wavelet coefficients of the three primary colors at each point of the image grid into a quartet of (o_1, o_2, o_3, o_4):

$$\begin{pmatrix} o_1 \\ o_2 \\ o_3 \\ o_4 \end{pmatrix} = \mathbf{R}_F \cdot \begin{pmatrix} r \\ g \\ b \end{pmatrix} = \begin{pmatrix} 1 & 1 & 1 \\ 1 & -1 & 0 \\ 0 & 1 & -1 \\ -1 & 0 & 1 \end{pmatrix} \cdot \begin{pmatrix} r \\ g \\ b \end{pmatrix}, \tag{1}$$

and then we apply the soft shrinkage with the threshold parameter $\mu_{+(n)}$ to o_1, whereas we apply the soft shrinkage with the threshold parameter $\mu_{-(n)}$ to o_2, o_3, and o_4 [3]. The two threshold parameters, $\mu_{+(n)}$, $\mu_{-(n)}$, of the soft shrinkage are defined as functions of the iteration parameter n:

$$\mu_{\pm(n)} = \mu_{\pm} \times \frac{(N_{\max} - n)}{(N_{\max} - 1)}, \quad n = 1, 2, \cdots, N_{\max}, \tag{2}$$

$N_{\max}$: Maximun number of iterations.

Finally, the four shrunken components $\{\hat{o}_1, \hat{o}_2, \hat{o}_3, \hat{o}_4\}$ are inversely transformed into the primary colors:

$$\begin{pmatrix} \hat{r} \\ \hat{g} \\ \hat{b} \end{pmatrix} = \mathbf{R}_I \cdot \begin{pmatrix} \hat{o}_1 \\ \hat{o}_2 \\ \hat{o}_3 \\ \hat{o}_4 \end{pmatrix} = \frac{1}{3} \begin{pmatrix} 1 & 1 & 0 & -1 \\ 1 & -1 & 1 & 0 \\ 1 & 0 & -1 & 1 \end{pmatrix} \cdot \begin{pmatrix} \hat{o}_1 \\ \hat{o}_2 \\ \hat{o}_3 \\ \hat{o}_4 \end{pmatrix}. \tag{3}$$

The matrix $\mathbf{R}_I$ is the least squares generalized inverse matrix.

3) Inverse SI-HWT:

We apply the inverse SI-HWT with three-resolution layers, and

thus we produce the n-th iterated demosaicked color image $\mathbf{F}^{(n)}$.

4) Clipping of the n-th iterated demosaicked color image $\mathbf{F}^{(n)}$:

We clip each color sample value of the n-th iterated demosaicked color image $\mathbf{F}^{(n)}$ within the dynamic range between 0 and 255 with the following scalar function:

$$f_{CL}(x) = \begin{cases} 0 \ , & if\ x < 0, \\ x \ , & if\ x \in [0, 255], \\ 255 \ , & if\ x > 255. \end{cases} \tag{4}$$

5) Convergence test:

If $\|\mathbf{F}^{(n)} - \mathbf{F}^{(n-1)}\|_2 < T_h$, then we will stop the iteration, and we will output the $\mathbf{F}^{(n)}$ as a finally-demosaicked color image; otherwise we will proceed to the step 6).

6) Forward SI-HWT with one resolution-layer:

We apply the forward SI-HWT with one resolution-layer to the n-th iterated demosaicked color image $\mathbf{F}^{(n)}$, and thus we produce the four bands, $L_1L_1^{(n+1)}$, $L_1H_1^{(n+1)}$, $H_1L_1^{(n+1)}$, $H_1H_1^{(n+1)}$. We update the iteration parameter n as $n \leftarrow n+1$.

7) Update of the scaling coefficients in the band $L_1L_1^{(n)}$:

We update the scaling coefficients, $r^{(n)}$, $g^{(n)}$, $b^{(n)}$, of the primary colors in the n-th iterated band $L_1L_1^{(n)}$ at only the points corresponding to observed color samples in the mosaicked image $\mathbf{I}_{mos}$:

$$\begin{cases} r^{(n)} \leftarrow r^{(n)} + 2 \cdot (2 \times r_{mos} - r^{(n)}), \\ g^{(n)} \leftarrow g^{(n)} + 2 \cdot (2 \times g_{mos} - g^{(n)}), \\ b^{(n)} \leftarrow b^{(n)} + 2 \cdot (2 \times b_{mos} - b^{(n)}), \end{cases} \tag{5}$$

where r_{mos}, g_{mos}, and b_{mos} are observed color sample values of the mosaicked image $\mathbf{I}_{mos}$.

8) Forward SI-HWT with two-resolution layers:

We apply the forward SI-HWT with two resolution-layers to the n-th iterated band $L_1L_1^{(n)}$, and thus we produce the seven bands, $L_3L_3^{(n)}$, $L_2H_2^{(n)}$, $H_2L_2^{(n)}$, $H_2H_2^{(n)}$, $L_3H_3^{(n)}$, $H_3L_3^{(n)}$, $H_3H_3^{(n)}$; and then we return to the step 2). [End of the algorithm]

4.2 Algorithm for the complementary CFA

The computational algorithm for the complementary CFA is identical to that for the primary CFA, except that the update of the scaling coefficients of the primary colors in the band L_1L_1, viz. the step 7) of the above-mentioned computational algorithm, is different between the cases of the complementary CFA and the primary CFA. Figure 4 illustrates an example of the update of the scaling coefficients of the primary colors in the band L_1L_1 for the complementary YMCG CFA. When an observed color sample is magenta, its magenta value $M^{(n)}$ is defined as an average of red and blue values, $r^{(n)}$, $b^{(n)}$, and hence at the same location of the image grid the red and the blue scaling coefficients in the L_1L_1 band are updated by

$$\begin{cases} r^{(n)} \leftarrow r^{(n)} + 2 \cdot (2 \cdot M_{mos} - M^{(n)}) \\ b^{(n)} \leftarrow b^{(n)} + 2 \cdot (2 \cdot M_{mos} - M^{(n)}) \end{cases} \tag{6}$$

where M_{mos} is an observed magenta sample value.

5. BASICS OF OUR ITERATIVE SHARPENING-DEMOSAICING APPROACH

This section addresses the issue of the theoretical foundation on which the above-mentioned computational algorithm of our sharpening-demosaicing approach is constructed.

5.1 Linear constraint on the coefficient vector of the SI-HWT

Assuming that primary color signals $\mathbf{F} = \{F_c \mid c = r, g, b\}$ with K by K pixels are represented as N (=K^2)-dimensional image vectors $\{\mathbf{f}_c \mid c = r, g, b\}$, the 2-D L-resolution-layer SI-HWT of each primary color signal will give $3LN$ wavelet coefficients and N scaling coefficients, and those coefficients will be collectively expressed as the $(3L+1)N$-dimensional coefficient vector $\mathbf{p}_c$. In the following, the sub-index c denoting a specific primary color channel is omitted and $(3L+1)$ is simply denoted by M; the image vector and the coefficient vector are simply represented by $\mathbf{f}$ and $\mathbf{p}$, respectively.

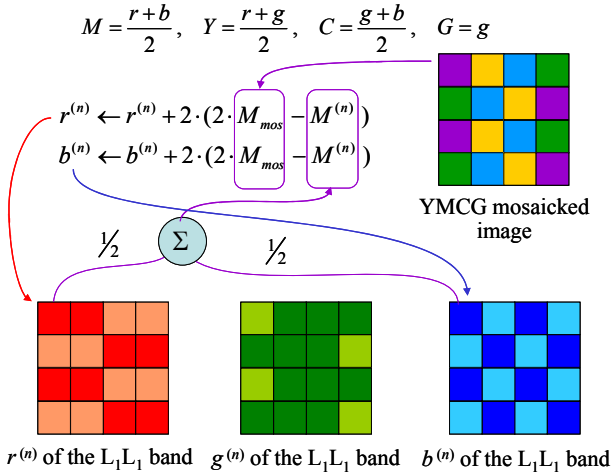

Figure 4 – Update of the scaling coefficients of the primary colors in the L_1L_1 band for the complementary YMCG CFA.

Under the above notation, the forward SI-HWT of $\mathbf{f}$ is expressed as

$$\mathbf{p} = \mathbf{T} \cdot \mathbf{f}, \quad \mathbf{T} : MN \times N \text{ transformation matrix}. \tag{7}$$

The inverse SI-HWT of ρ is expressed as

$$\mathbf{f} = \mathbf{D} \cdot \mathbf{p}, \quad \mathbf{D} : N \times MN \text{ dictionary matrix}. \tag{8}$$

Between the transformation matrix $\mathbf{T}$ and the dictionary matrix $\mathbf{D}$, the following properties hold true:

$$\mathbf{D} \cdot \mathbf{T} = \mathbf{I}_N, \quad \mathbf{I}_N : N \times N \text{ identity matrix}, \tag{9}$$

$$\mathbf{D} = \mathbf{T}^+ = (\mathbf{T}^{\mathrm{T}} \cdot \mathbf{T})^{-1} \cdot \mathbf{T}^{\mathrm{T}}, \quad \mathbf{T} = \mathbf{D}^+ = \mathbf{D}^{\mathrm{T}} \cdot (\mathbf{D} \cdot \mathbf{D}^{\mathrm{T}})^{-1} \tag{10}$$

The dictionary matrix $\mathbf{D}$ is a left-inverse matrix of the transformation matrix $\mathbf{T}$. As the coefficient vector $\mathbf{p}$, we cannot freely choose an arbitrary vector from the MN-dimensional linear space. The coefficient vector $\mathbf{p}$ should lie in a certain N-dimensional linear subspace embedded in the MN-dimensional linear space. To clarify this linear constraint, we map $\mathbf{p}$ through the application of the inverse SI-HWT followed by the application of the forward SI-HWT:

$$\mathbf{p} \xrightarrow[\mathbf{D}]{\text{Inverse SI-HWT}} \tilde{\mathbf{f}} \xrightarrow[\mathbf{T}]{\text{Forward SI-HWT}} \tilde{\mathbf{p}}. \tag{11}$$

These procedures correspond to the concatenation of the step 3) and the step 6) and the step 8). The mapping from $\mathbf{p}$ to $\tilde{\mathbf{p}}$ is represented simply by the linear transformation:

$$\tilde{\mathbf{p}} = \mathbf{T} \cdot \mathbf{D} \cdot \mathbf{p}. \tag{12}$$

We define the matrix $\mathbf{Q}$ by

$$\mathbf{Q} = \mathbf{T} \cdot \mathbf{D}. \tag{13}$$

The rank of the MN by MN matrix $\mathbf{Q}$ is N, and the matrix $\mathbf{Q}$ is singular. The matrix $\mathbf{Q}$ has the following properties: 1) the idempotency, $\mathbf{Q}^2 = \mathbf{Q}$, and 2) the symmetry, $\mathbf{Q}^{\mathrm{T}} = \mathbf{Q}$. Hence, the linear mapping by $\mathbf{Q}$ means the orthogonal projection onto the N-dimensional column-space of $\mathbf{Q}$:

$$\tilde{\mathbf{p}} = \mathrm{P}_{\mathbf{Q}}(\mathbf{p}) = \mathbf{Q} \cdot \mathbf{p}, \tag{14}$$

$$: \text{Orthogonal projection of } \mathbf{p} \text{ onto } \mathbf{R}(\mathbf{Q}),$$

$$\mathbf{R}(\mathbf{Q}) : N\text{-dimmensional column-sapce of } \mathbf{Q}.$$

The above means that $\mathbf{p}$ has redundancy and the consistent coefficient-vector $\mathbf{p}$ always satisfies the linear constraint that it should belong to the N-dimensional column-space of $\mathbf{Q}$.

5.2 Clipping of each color sample value

The clipping of each color sample value of the color image $\mathbf{f} = \mathbf{D} \cdot \mathbf{p}$

performed at the step 4) is equivalent to the convex projection of $\mathbf{f}$ onto the convex set $\mathbf{C}_R$ that each color sample value of a color image belonging to the set should lie between 0 and 255.

5.3 Update of the scaling coefficients in the L_1L_1 band

We define the matrix $\mathbf{E}$ to generate the N scaling coefficients, r, g, b, of the primary colors at in the L_1L_1 band at only the points corresponding to observed color samples in the mosaicked image $\mathbf{I}_{mos}$, from the three MN-dimensional coefficient vectors $(\mathbf{p}_c \mid c = r, g, b\}$, as follows:

$$\mathbf{g} = \mathbf{E} \cdot \mathbf{p}_{rgb}, \qquad \mathbf{p}_{rgb} = \left(\mathbf{p}_r^{\mathrm{T}} \quad \mathbf{p}_g^{\mathrm{T}} \quad \mathbf{p}_b^{\mathrm{T}}\right)^{\mathrm{T}} \tag{15}$$

$\mathbf{g} \in \mathbf{R}^N$: Vector composed of the selected N scaling coefficients,

$\mathbf{E}$: $N \times 3MN$ matrix to generate $\mathbf{g}$ from $\{\mathbf{p}_R, \mathbf{p}_G, \mathbf{p}_B\}$.

Under this notation, we define the set $\mathbf{C_s}$ satisfying the constraint that the generated N scaling coefficients $\mathbf{g}$ in the L_1L_1 band should coincide with double the observed N color samples $\mathbf{s}$ of the mosaicked image $\mathbf{I}_{mos}$, as follows:

$$\mathbf{C_s} = \left\{\mathbf{p}_{rgb} \,\middle|\, \mathbf{g} = \mathbf{E} \cdot \mathbf{p}_{rgb} = 2 \cdot \mathbf{s}, \mathbf{p}_{rgb} \in \mathbf{R}^{3MN}, \mathbf{g} \in \mathbf{R}^N, \mathbf{s} \in \mathbf{R}^N\right\}. \tag{16}$$

The constraint set $\mathbf{C_s}$ is convex, and the convex projection $P_{\mathbf{C_s}}$ of $\mathbf{p}_{rgb}$ onto $\mathbf{C_s}$ is simply performed by replacing the selected scaling coefficients $\mathbf{g}$ of $\mathbf{p}_{rgb}$ with double the observed N color samples $\mathbf{s}$ of the mosaicked image $\mathbf{I}_{mos}$, and simultaneously keeping the other coefficients of $\mathbf{p}_{rgb}$ unchanged. On the other hand, in the step 7), to accelerate the convergence of the iterative algorithm, instead of the simple convex projection we adopt the update procedure of (5). The update procedure of (5) means the following mapping:

$$\hat{\mathbf{p}}_{rgb} = \mathbf{p}_{rgb} + 2 \cdot \left\{P_{\mathbf{C_s}}\left(\mathbf{p}_{rgb}\right) - \mathbf{p}_{rgb}\right\} = 2 \cdot P_{\mathbf{C_s}}\left(\mathbf{p}_{rgb}\right) - \mathbf{p}_{rgb} \tag{17}$$

This mapping is non-expansive; and its iterative application renders its mapped vector to converge on a fixed point, identical to the convex projection $P_{\mathbf{C_s}}(\mathbf{p}_{rgb})$.

5.4 Convergence of the iterative algorithm

The color shrinkage with the redundant color transform of (1) in the step 2) is regarded as a close approximation of our previously proposed soft color-shrinkage [8]. We represent the mosaicked image and the n-th iterated color-image inputted to the step 2), simply by $\mathbf{I}_{mos}$, and $\mathbf{F}^{(n)} = \{\mathbf{R}', \mathbf{G}', \mathbf{B}'\}$, respectively; and we represent three-resolution-layer SI-HWT coefficient vectors of a color image $\mathbf{F} = \{\mathbf{R}, \mathbf{G}, \mathbf{B}\}$ by $\mathbf{p}_{rgb} = \{\mathbf{p}_r, \mathbf{p}_g, \mathbf{p}_b\}$. Moreover, we represent a color-image $\mathbf{F}$ in the redundant color space by $\mathbf{F} = \{\mathbf{O}_1, \mathbf{O}_2, \mathbf{O}_3, \mathbf{O}_4\}$, and we define the Besov-type norm of $\mathbf{F}$ in the SI-HWT transform domain of the four redundant color components, $\mathbf{O}_1$, $\mathbf{O}_2$, $\mathbf{O}_3$, $\mathbf{O}_4$. Under this notation, we formulate a denoising-type variational problem with the Besov-type energy function $E'(\mathbf{F}|\mathbf{F}^{(n)})$ defined in the redundant color space of (1):

$$\mathbf{F}^* = \arg \min_{\mathbf{F}=\{\mathbf{O}_1,\mathbf{O}_2,\mathbf{O}_3,\mathbf{O}_4\}} \{E'(\mathbf{F} \mid \mathbf{F}^{(n)})\}, \tag{18}$$

$$E'(\mathbf{F} \mid \mathbf{F}^{(n)}) = E_B(\mathbf{F}) + \frac{\lambda_+}{2} \| \mathbf{O}_1 - (\mathbf{R}' + \mathbf{G}' + \mathbf{B}') \|_2^2$$

$$+ \frac{\lambda_-}{2}\left\{\|\mathbf{O}_2 - (\mathbf{R}' - \mathbf{G}')\|_2^2 + \|\mathbf{O}_3 - (\mathbf{G}' - \mathbf{B}')\|_2^2 + \|\mathbf{O}_4 - (\mathbf{B}' - \mathbf{R}')\|_2^2\right\},$$

$$E_B(\mathbf{F}) = \|\mathbf{O}_1\|_{B^1_{1,1}} + \|\mathbf{O}_2\|_{B^1_{1,1}} + \|\mathbf{O}_3\|_{B^1_{1,1}} + \|\mathbf{O}_4\|_{B^1_{1,1}},$$

$\|*\|_{B^1_{1,1}}$: (1,1,1)-type Besov norm, $\lambda_+ > 0$, $\lambda_- > 0$,

where the (1, 1, 1)-type Besov norm is defined as the sum of the l^1 norm of the wavelet coefficients, and well approximates the TV norm [7]. The output of the color shrinkage in the redundant color space at the n-th iteration can be interpreted as the unique solution $\mathbf{F}^*$ of (18), and hence the following inequality holds true:

$$E'(\mathbf{F}^* \mid \mathbf{F}^{(n)}) \le E'(\mathbf{F}^{(n)} \mid \mathbf{F}^{(n)}). \tag{19}$$

From (18), it is proved that the following inequality holds true:

$$E_B(\mathbf{F}^*) \le E_B(\mathbf{F}^{(n)}). \tag{20}$$

This inequality reveals that the iterative algorithm minimizes the Besov-type energy function E_B of an output color-image $\mathbf{F}$ subject to the linear constraint on the coefficient vector $\mathbf{p}_{rgb}$ of the SI-HWT, the convex constraint on the dynamic range of each color sample value of the output color image $\mathbf{F} = \mathbf{D} \cdot \mathbf{p}_{rgb}$, and the convex constraint on the selected N scaling coefficients $\mathbf{g}$ of the coefficient vector $\mathbf{p}_{rgb}$. Therefore, the iterative algorithm is interpreted as a solver of the constrained variational image-restoration problem:

$$\min_{\mathbf{F}=\{\mathbf{O}_1,\mathbf{O}_2,\mathbf{O}_3,\mathbf{O}_4\}} E_B(\mathbf{F}) \tag{21}$$

, subject to $\boldsymbol{\rho}_{rgb} \in \mathbf{C_s}$, $\mathbf{H} = \mathbf{D} \cdot \boldsymbol{\rho}_{rgb} \in \mathbf{C}_R$, and $\boldsymbol{\rho}_{rgb} \in \mathbf{R}(\mathbf{Q})$.

Since the variational problem of (21) is a convex optimization problem subject to the three different bounded closed convex constraints, an optimal solution of (21) necessarily exists, and is uniquely determined. The algorithm alternately iterates the three procedures: the concatenation of the inverse SI-HWT and the forward SI-HWT with three resolution-layers, the convex projection onto the convex set $\mathbf{C}_R$, the non-expansive mapping constructed from the convex projection onto the convex set $\mathbf{C_s}$, and the color shrinkage of the wavelet coefficients, and thus it iteratively solves (21). This iterative solver is equivalent to the hybrid steepest descent (HSD) solver [9]. According to the strong convergence theorem of the HSD solver [9], under the scheme of (2) to control the two threshold parameters, $\mu_{+(n)}$, $\mu_{-(n)}$, of the color shrinkage according as the iteration parameter n goes to N_{max}, if N_{max} is sufficiently large, then the n-th iterated demosaicked color image $\mathbf{F}^{(n)}$ will necessarily converge to the unique optimal solution, determined by the mosaicked image $\mathbf{I}_{mos}$.

6. EXPERIMENTAL SIMULATIONS

To evaluate the demosaicing performance, we use KODAK standard color images. Fig. 5 shows the set of the 24 original color images. The test mosaicked images are artificially produced by applying to the KODAK standard color images both the low-pass filtering of Fig. 2(a) mimicking the O-LPF and the color-mosaicing with a certain CFA, shown in Fig. 6, namely the Bayer's CFA, the complementary YMCG CFA [4], the random arrangement primary CFA (RGB random CFA) [5], [6] where the ratio of the three primary color sensors is set to R : G : B = 1 : 1 : 1, and the random arrangement complementary CFA (YMC random CFA) where the ratio of the three complementary color sensors is set to Y : M : C = 1 : 1 : 1. The RGB random CFA simulates the color mosaicing performed by a retina of an eye. Using these mosaicked test images, we compare the four types of CFA in PSNR [dB] of color images restored by our newly proposed iterative sharpening-demosaicing method with the SI-HWT (SD-SIHWT). Moreover, in the case of the Bayer's CFA, we compare demosaicing performance of our previously proposed iterative sharpening-demosaicing method with the TV regularization in the spatial image-domain (SD-TV) [1] and that of our new SD-SIHWT.

6.1 SD-SIHWT vs. SD-TV

The two maximum values, μ_+, μ_-, of the threshold parameters of the color shrinkage are experimentally optimized for the image set of Fig. 5, and their optimized values are $\mu_+ = 0.975$ and $\mu_- = 2.608$. The parameters of the SD-TV are optimized in a similar way. Table 1 compares PSNR'*s* of color images restored by the SD-SIHWT and the SD-TV; in all the experimental simulations the maximum iteration number *Nmax* is fixed at 200. The PSNR'*s* of Table 1 are total PSNR'*s* computed for the image set of Fig. 5. The SD-SIHWT outperforms the SD-TV by approximately 3.3 [dB].

6.2 Four different type of CFA

For the 24 images of Fig. 5, Fig. 7 shows PSNR'*s* of color images recovered by our SD-SIHWT, in the cases of the four different

CFA'*s* of Fig. 6, and Fig. 8 compares color images recovered by the SD-SIHWT. As for the PSNR'*s*, the YMCG CFA achieves the best performance, second to it the YMC random CFA performs best, and the Bayer's CFA ranks third; but in the white-fence image region of Fig. 8 the Bayer's CFA produces diffused false color artifacts, whereas the YMCG CFA produces artificial small color patterns with high color saturation. The random arrangement CFA'*s* yield recovered color images with PSNR comparable to the cases of their corresponding regular arrangement CFA'*s* such as the Bayer's CFA; but, as shown in Fig. 8, they tend to suppress false-color artifacts a little better than their corresponding regular arrangement CFA'*s*.

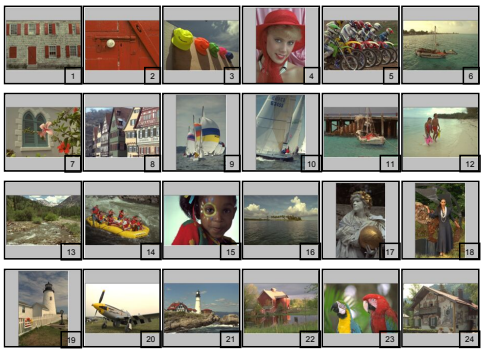

Figure 5 – Set of the 24 original color images.

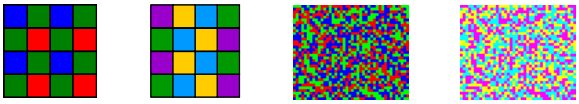

(a) (b) (c) (d)

Figure 6 – Four types of CFA: (a) Bayer's CFA, (b) YMCG CFA, (c) Random arrangement primary CFA (RGB random CFA), (d) Random arrangement complementary CFA (YMC random CFA).

Table 1 – Total PSNR'*s* of recovered color images.

Method	SD-SIHWT	SD-TV
PSNR [dB]	37.4	34.1

7. CONCLUSIONS

Extending the monochrome-image deblurring method [2], we present an iterative sharpening-demosaicing approach with the shift-invariant Haar wavelet transform and our color shrinkage utilizing redundant color transformation [3]. Our new method works more efficiently than our previously proposed sharpening-demosaicing method with the spatial TV regularization [1], and it recovers high-quality color images for various types of CFA. However, our new method requires more than one hundred iterations for its convergence, and its computational complexity is very high. Hence, we need to develop a method to accelerate its convergence.

REFERENCES

[1]T. Komatsu and T. Saito, "Sharpening-demosaicing method using the total-variation regularization," *J. ITE Japan*, vol.61, no.11, pp.1621-1632, Nov. 2007.

[2]R. H. Chan, T. F. Chan, L. Shen, and Z. Shen, "Wavelet algorithms for high-resolution image reconstruction," *SIAM J. Sci. Comput.*, vol. 24, no. 4, pp.1408–1432, Feb. 2003.

[3]T. Saito, Y. Ueda, and T. Komatsu, "Color shrinkage for sparse coding of color images," *EUSIPCO 2010* (to be submitted).

[4]K. Hirakawa and P.J. Wolfe, "Spatio-spectral color filter array design for enhanced image fidelity," in *Proc. 2007 IEEE Int. Conf. on Image Process.*, Sept. 2007, pp.1183-1184.

[5]R. Likac and K. N. Plataniotis, "Color filtrer array: design and performance analysis," *IEEE Trans. Consumer Electron.*, vol.51, no.4, pp.1260-1267, Nov. 2005.

[6]L. Condat, "A new random color filter array with good spectral properties," in *Proc. 2009 IEEE Int. Conf. on Image Process.*, Nov. 2009, pp.1613-1616.

[7]A. Chambolle, R.A. De Vore, N. Lee, and B.J. Lucier, "Nonlinear wavelet image processing: variational problems, compression, and noise removal through wavelet shrinkage," *IEEE Trans. Image Process.*, vol.7, no.3, pp.319-335, Mar. 1998.

[8]T. Saito, N. Fujii, and T. Komatsu, "Iterative soft color-shrinkage for color-image denoising," in *Proc. 2009 IEEE Int. Conf. on Image Process.*, Nov. 2009, pp.3837-3840.

[9]I. Yamada, "The hybrid steepest descent method for the variational inequality problem over the intersection of fixed points sets of nonexpansive mappings," in *Inherently Parallel Algorithm in Feasibility and Optimization and their Applications*, pp.473-504: Elsevier, New York, 2001.

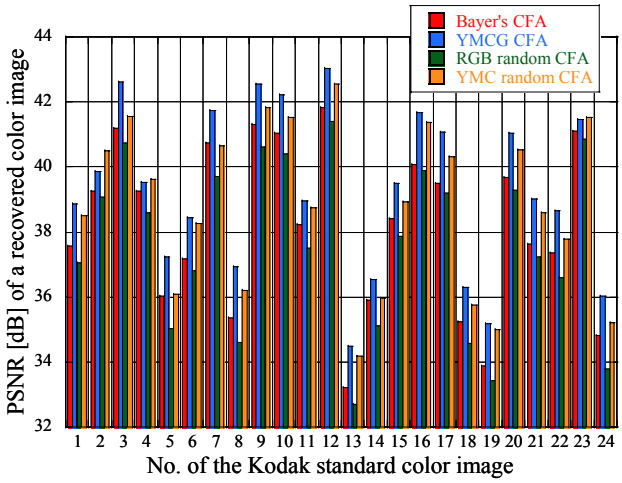

Figure 7 – PSNR'*s* of color images recovered by the SD-SIHWT in the cases of the four different CFA types of Fig. 6.

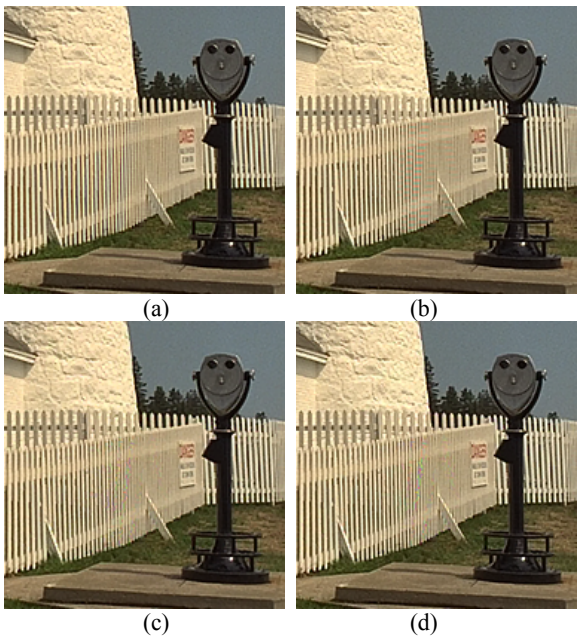

(a) (b) (c) (d)

Figure 8 – Color images recovered by the SD-SIHWT: (a) Bayer's CFA, (b) YMCG CFA, (c) Random arrangement primary CFA, (d) Random arrangement complementary CFA.